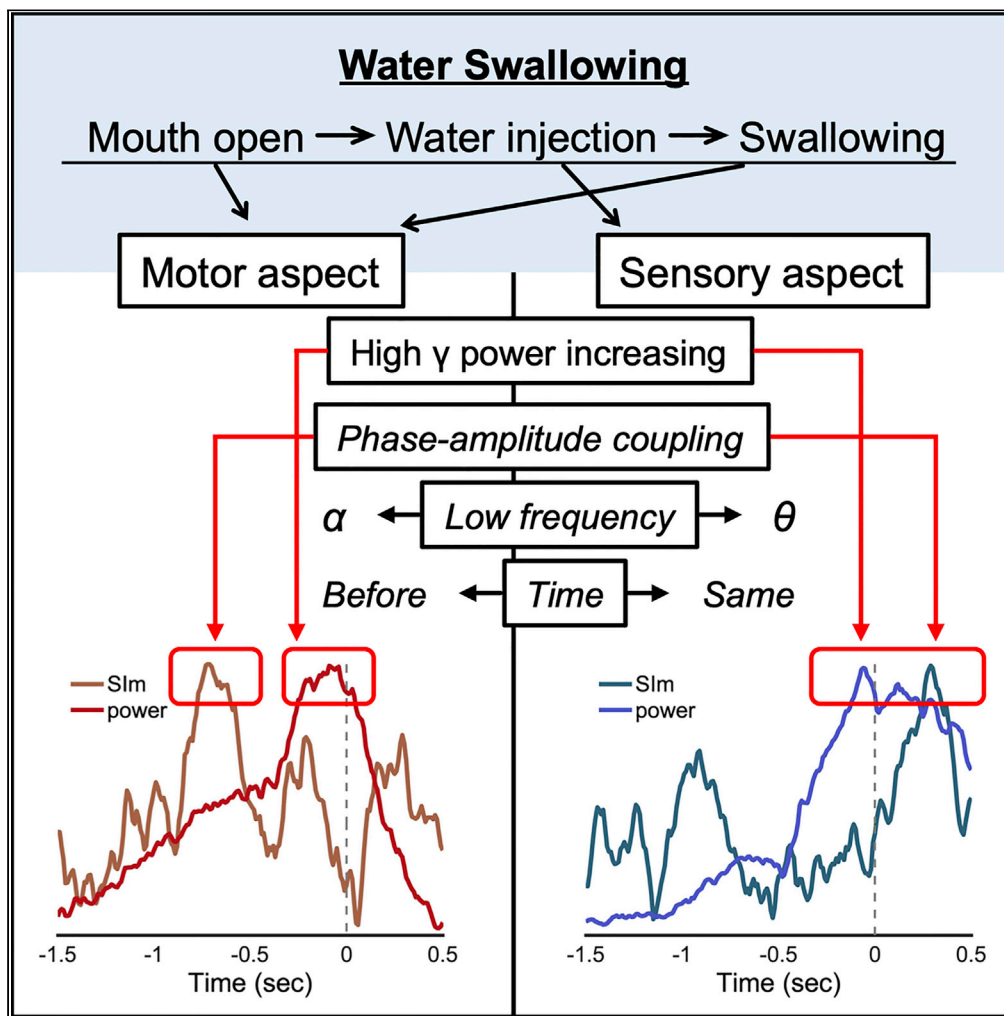**Article**

Motor and sensory cortical processing of neural oscillatory activities revealed by human swallowing using intracranial electrodes

Hiroaki Hashimoto, Kazutaka Takahashi, Seiji Kameda, ..., Toshiki Yoshimine, Haruhiko Kishima, Masayuki Hirata

h-hashimoto@ndr.med.
osaka-u.ac.jp (H.H.)
mhirata@ndr.med.osaka-u.ac.
jp (M.H.)

Highlights

Swallowing has two aspects; sensory input and motor output

Phase-amplitude coupling showed differences of motor and sensory neural processing

Coupling between the α and high γ band occurred before motor-related high γ activities

Coupling between the θ and high γ band occurred during sensory-related high γ activities

iScience

Article

Motor and sensory cortical processing of neural oscillatory activities revealed by human swallowing using intracranial electrodes

Hiroaki Hashimoto,[1,2,3,*] Kazutaka Takahashi,[4] Seiji Kameda,[1] Fumiaki Yoshida,[1,5] Hitoshi Maezawa,[1] Satoru Oshino,[6] Naoki Tani,[6] Hui Ming Khoo,[6] Takufumi Yanagisawa,[6] Toshiki Yoshimine,[3] Haruhiko Kishima,[6] and Masayuki Hirata[1,3,6,7,*]

SUMMARY

Swallowing is attributed to the orchestration of motor output and sensory input. We hypothesized that swallowing can illustrate differences between motor and sensory neural processing. Eight epileptic participants fitted with intracranial electrodes over the orofacial cortex were asked to swallow a water bolus. Mouth opening and swallowing were treated as motor tasks, whereas water injection was treated as a sensory task. Phase-amplitude coupling between lower-frequency and high γ (HG) bands (75–150 Hz) was investigated. An α (10–16 Hz)-HG coupling appeared before motor-related HG power increases (burst), and a θ (5–9 Hz)-HG coupling appeared during sensory-related HG bursts. The peaks of motor-related coupling were 0.6–0.7 s earlier than that of HG power. The motor-related HG was modulated at the trough of the α oscillation, and the sensory-related HG amplitude was modulated at the peak of the θ oscillation. These contrasting results can help to elucidate the brain's sensory motor functions.

INTRODUCTION

Motor- and sensory-related tasks induce neural oscillatory changes in the cortex. During movement or stimulation task activating the sensorimotor cortex, power suppression of beta band was observed (Pfurtscheller, 1981). Suppressed β bands are re-activated following the completion of motor task, which is referred to as the "rebound β" (Salmelin and Sams, 2002). Oscillatory changes related to sensory stimulation have been reported in a magnetoencephalography (MEG) study (Hirata et al., 2002; Maezawa et al., 2008). These frequency bands, i.e., the α (8–14 Hz) (Haegens et al., 2011) and β (15–25 Hz) (Crone et al., 1998b), are lower-frequency bands (Miller et al., 2007), whereas frequencies over 30 Hz are γ bands and those >75 Hz are referred to as high γ (HG) band (Crone et al., 1998a).

HG activities are involved in not only sensory (Hirata et al., 2002) and motor tasks (Crone et al., 1998a; Dalal et al., 2008) but also attention (Taylor et al., 2005), language (Hashimoto et al., 2017), and working memory (Pipa et al., 2009). Recently, the MEG study showed that HG activities were induced by the sensory stimulation of the pharynx (Muhle et al., 2021). HG activity is a key oscillation that reflects the neural processing and shows better functional localization than lower-frequency activity (Canolty et al., 2006; Crone et al., 1998a; Miller et al., 2007). HG activities are physiological activities; pathological high-frequency activities (HFAs) have been reported in epilepsy (Ayoubian et al., 2013; Hashimoto et al., 2021a; Jacobs et al., 2009; Matsumoto et al., 2013).

The relationship between the high- and low-frequency activities has been investigated using phase-amplitude coupling (PAC) methods (Cohen, 2008). PAC showed that the amplitude of HG activities was modulated by a phase of low-frequency oscillations (Canolty et al., 2006). PAC plays different functional roles in cortical processing, such as motor execution (Yanagisawa et al., 2012b) and somatosensory processing (Lakatos et al., 2008). PAC is thought to be related to physiological neural processing, whereas PAC has also been reported to be associated with pathological neural processing, such as epileptic seizures (Hashimoto et al., 2020b, 2021a) and Parkinson's disease (de Hemptinne et al., 2015).

[1]Department of Neurological Diagnosis and Restoration, Graduate School of Medicine, Osaka University, Yamadaoka 2-2, Suita, Osaka 565-0871, Japan

[2]Department of Neurosurgery, Otemae Hospital, Chuo-ku Otemae 1-5-34, Osaka, Osaka 540-0008, Japan

[3]Endowed Research Department of Clinical Neuroengineering, Global Center for Medical Engineering and Informatics, Osaka University, Yamadaoka 2-2, Suita, Osaka 565-0871, Japan

[4]Department of Organismal Biology and Anatomy, The University of Chicago, 1027 E 57th St, Chicago, IL 60637, USA

[5]Department of Anatomy and Physiology, Saga Medical School Faculty of Medicine, Saga University, Nabeshima 5-1-1, Saga, Saga 849-8501, Japan

[6]Department of Neurosurgery, Graduate School of Medicine, Osaka University, Yamadaoka 2-2, Suita, Osaka 565-0871, Japan

[7]Lead contact

*Correspondence:
h-hashimoto@ndr.med.osaka-u.ac.jp (H.H.),
mhirata@ndr.med.osaka-u.ac.jp (M.H.)

https://doi.org/10.1016/j.isci.2021.102786

Some studies regarding the above neural oscillations were investigated for clinical applications. The lower-frequency neural oscillations in the sensorimotor cortex measured by scalp electroencephalogram (EEG) were used for decoding in rehabilitation using brain-machine interface techniques (Ramos-Murguialday et al., 2013; Shindo et al., 2011), whereas HG activities could be used to decode more accurate, rather than lower, frequency bands (Hashimoto et al., 2020a; Yanagisawa et al., 2011, 2012a). PAC could be used to detect or predict epileptic seizures (Amiri et al., 2019; Edakawa et al., 2016).

To investigate motor- and sensory-related neural oscillations, various tasks have been used including motor-related tasks, such as button pressing (Pfurtscheller and Aranibar, 1979), hand and elbow movements (Yanagisawa et al., 2012a), and tongue movements (Miller et al., 2007), as well as sensory-related tasks, such as median nerve stimulation (Hirata et al., 2002), tongue stimulation (Maezawa et al., 2008), buccal mucosa stimulation (Miyaji et al., 2014), and pharyngeal electrical stimulation (Muhle et al., 2021). Even swallowing is used as a task to investigate neural oscillatory changes (Cuellar et al., 2016; Dziewas et al., 2003; Furlong et al., 2004; Satow et al., 2004).

Swallowing is executed by cooperation between multiple regions of the cerebral cortex and the brainstem (Ertekin and Aydogdu, 2003). Noninvasive methods, such as scalp EEG (Yang et al., 2014), positron emission tomography (Hamdy et al., 1999b), near-infrared spectroscopy (Kober and Wood, 2014), transcranial magnetic stimulation (Hamdy et al., 1996), functional magnetic resonance imaging (Hamdy et al., 1999a; Toogood et al., 2017), and MEG (Dziewas et al., 2003; Furlong et al., 2004) implicate multiple cortical sites involved in swallowing. Invasive methods like intracranial EEG (iEEG) were also used in combination with the swallowing task (Satow et al., 2004). Swallowing is a unique movement because cooperation between voluntary and involuntary movements is necessary for normal swallowing. Therefore, swallowing is divided into two components: voluntary and involuntary movement (Jean, 2001). Our iEEG study showed that HG activities in the cortex along the Sylvian fissure achieved the maximum values at the transition time from the voluntary to the involuntary phase (Hashimoto et al., 2021b).

Moreover, swallowing is a unique movement since cooperation between motor output and sensory input is involved. Sensory input is essential to the initiation and modulation of normal swallowing (Gow et al., 2004; Lowell et al., 2008); anesthesia of the oral and pharynx area can interfere with swallowing (Mårnsson and Sandberg, 1974). Various muscles of the oral area, pharynx, and esophagus are involved in swallowing execution (Ertekin and Aydogdu, 2003). Therefore, the swallowing water task has two aspects: a motor output aspect that includes mouth open and swallowing, whereas the other is a sensory input aspect that includes stimulation of the buccal mucosa by water injection into the oral cavity.

Here, we hypothesized that the swallowing water task can show differences between motor and sensory neural processing. This study has two aims: one, since the role of PAC in swallowing remains unknown, to determine whether PAC is observed during the swallowing task in the orofacial cortex, and two, to identify the differences between motor- and sensory-related neural processing using a combination of swallowing water task and PAC methods.

Neurophysiological recording techniques, such as iEEG or electrocorticogram, can identify neural oscillatory changes up to HG bands. In this study, we recorded iEEG signals in the orofacial cortex of patients with epilepsy (Figure 1) while swallowing a bolus of water. We continue to research for contributions to recovery from dysphagia using swallowing-related neural activities in combination with our brain-machine interface technology. As a part of this research, we have previously reported the development of a swallow-tracking system that enabled us to monitor swallowing noninvasively using Kinect v2 (Microsoft, Redmond, Washington, USA) (Hashimoto et al., 2018). We can use this swallow-tracking system simultaneously with iEEG measurement to detect the time when participants open their mouth, when water bolus was injected into the mouth, and when participants swallowed (Figure 2). Therefore, we could insert three different triggers into iEEG signals; mouth-triggers (Mouth-T), water-triggers (Water-T), and swallow-triggers (Swallow-T), which corresponded to the three different times, respectively. We have also analyzed the iEEG signals that are time locked to the triggers. Mouth-T and Swallow-T represented a motor task, whereas Water-T represented a sensory task. The synchronization index (SI) was used for PAC analysis (Cohen, 2008).
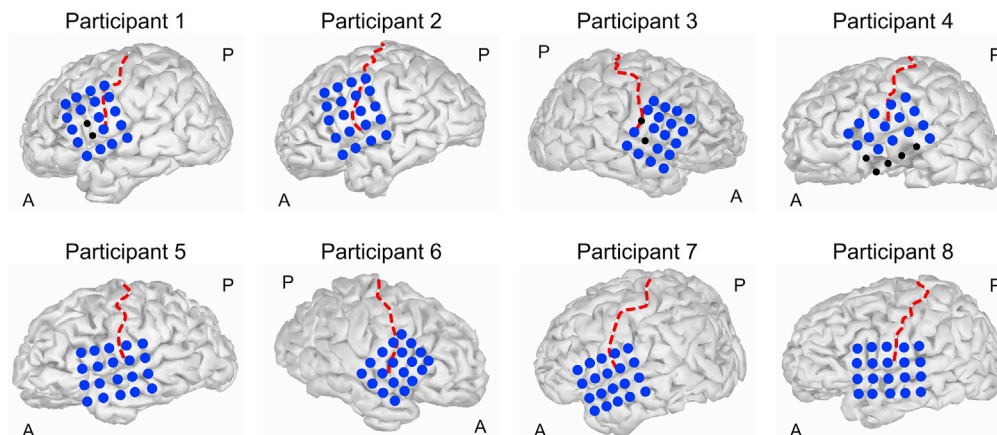
Figure 1. The location of the orofacial electrodes
The placements of the implanted electrodes of all participants are indicated. Black color indicates electrodes excluded from the analyses because of contamination such as severe noise or epileptic discharges. The central sulcus is indicated by the red dashed line. A, anterior; P, posterior.

RESULTS

Distribution of HG activities related to mouth opening, water injection, and swallowing

For a representative participant (Participant 1; P1), the spatial HG normalized power distributions in the orofacial cortex are shown in Figure 3A. Within three different triggers, including Mouth-T, Water-T, and Swallow-T, significant HG power increasing contacts (corrected p [c.p] < 0.05, single-sided permutation tests with Bonferroni correction) are indicated as filled white circles, and we could observe a different spatial distribution.

### Distribution of contacts indicating significant HG increase

A total of eight participants were enrolled (Table 1), and the patient group in this study was the same as that used in our other published study (Hashimoto et al., 2020a, 2021b). All contacts showing HG power increase in eight participants were plotted on the left hemisphere of the Montreal Neurological Institute (MNI) normalized brain (Figure 3B). For better distribution clarity, the contacts attached to the right hemisphere were transposed to the left hemisphere. Next, we selected the contacts indicating the maximum values of significant HG power increase within Mouth-T, Water-T, and Swallow-T from each participant, and the total eight contacts within each trigger were plotted on the left hemisphere of the MNI normalized brain (Figure 3C). With Mouth-T, HG increase was observed primarily in the frontal lobe, and with Water-T, HG increase was observed in the lateral pericentral gyri. With Swallow-T, HG increase appeared in the region along the Sylvian fissure. These three groups were defined as a mouth contacts group (Mouth group), a water contacts group (Water group), and a swallow contacts group (Swallow group).

Temporal HG power changes

The averaged normalized power of HG around Mouth-T, Water-T, and Swallow-T was calculated from the Mouth (green), Water (blue), and Swallow groups (red) (Figure 4A). Around 0 s, the Mouth group with Mouth-T (green line in Figure 4A left panel) and the Swallow group with Swallow-T (red line in Figure 4A right panel) indicated notable HG power increases corresponding to motor-related HG activities. Although the Water group with Water-T also showed notable HG activities around 0 s (blue line in Figure 4A median panel), this was deemed to correspond to sensory-related HG activities.

HG amplitude coupled with lower-frequency phase

To investigate differences between motor- and sensory-related HG activities, we used PAC analysis with SI (Cohen, 2008). Since SI is a complex number, we used the magnitude of SI (SIm) in our calculations. SIm ranges between 0 and 1, with 0 indicating completely desynchronized phases and 1 indicating perfectly synchronized phases. We calculated SIm (Figure 4B) and normalized SIm (Figure 4C) with a combination of lower-frequency (5–30 Hz, 1 Hz bin) phase and fixed HG (75–150 Hz) amplitude. Before motor-related HG activities, high SIm and high normalized SIm were observed (Figures 4B and 4C left and right panels,
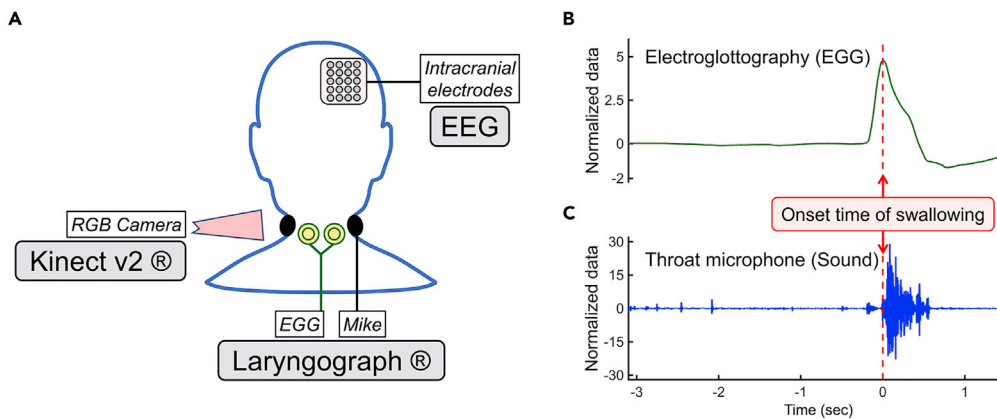
Figure 2. Swallowing monitoring

Intracranial electroencephalogram (EEG) was recorded during participants' swallowing. The swallowing was monitored by an RGB camera of Kinect v2 (Microsoft), an electroglottograph (EGG), and the microphone of a laryngograph (A). Across-trials averaged impedance waveforms of an EGG (B) and a throat microphone (sound) (C) from Participant 1 (P1) are shown. For analysis, the onset of swallowing was defined as the peak time of an impedance waveform. We could detect when participants opened their mouths and when water bolus was injected into the mouth by the RGB camera of Kinect v2.

red dashed square). On the contrary, during sensory-related HG activities, high SIm values were observed (Figure 4B median panel, red dashed square).

Profiles of motor- and sensory-related PAC

In motor- and sensory-related PAC, the main lower-frequency band indicating high values of SIm was under 20 Hz; therefore, we fixed the lower frequency range; 5–9 Hz was defined as representation of the θ band and 10–16 Hz of the α band. With Mouth-T, Water-T, and Swallow-T, dynamic changes of SIm between θ phase and HG amplitude, and α phase and HG amplitude were plotted using the Mouth (green), Water (blue), and Swallow groups (red) (Figure 5A).

In Mouth-T, α-HG SIm of the Mouth group showed a peak at −0.6 s (Figure 5A, top column, red arrow). Significant differences of α-HG SIm among the three groups were observed both before and during the HG burst (c.p < 0.05 and c.p < 0.01, respectively, one-way analysis of variance [ANOVA] with Bonferroni correction) (Figure 5A, top column, cyan and magenta mesh areas). In only before HG burst with α-HG SIm, the Mouth group reached significantly higher values than the other two groups (c.p < 0.05, t test with Bonferroni correction; Figure 5B, top column and red asterisk).

In Water-T, θ-HG SIm of the Water group showed a peak at 0.2 s (Figure 5A, middle column, red arrow). Significant differences among the three groups were observed during the HG burst both in θ-HG SIm and in α-HG SIm (c.p < 0.01, ANOVA with Bonferroni correction) (Figure 5A, middle column, magenta mesh area). In only θ-HG SIm during HG burst, the Water group reached significantly higher values than the other two groups (c.p < 0.01, t test with Bonferroni correction; Figure 5C, middle column and red asterisk).

In Swallow-T, α-HG SIm of the Swallow group showed a peak at −0.7 s (Figure 5A, bottom column, red arrow). Significant differences among the three contact groups were observed before the HG burst of α-HG SIm, during the HG bursts of θ-HG SIm, and α-HG SIm (c.p < 0.01, ANOVA with Bonferroni correction) (Figure 5A, bottom column, cyan and magenta mesh areas). Before HG burst with α-HG SIm, the Swallow group reached significantly higher values than the other two groups (c.p < 0.01, t test with Bonferroni correction; Figure 5B, bottom column and red asterisk).

We concluded that motor-related PAC appeared before motor-related HG burst, not during HG burst, and its main lower frequency phase was the α band (10–16 Hz), whereas the sensory-related PAC appeared during sensory-related HG burst and its main lower frequency phase was the θ band (5–9 Hz) (Table 2).
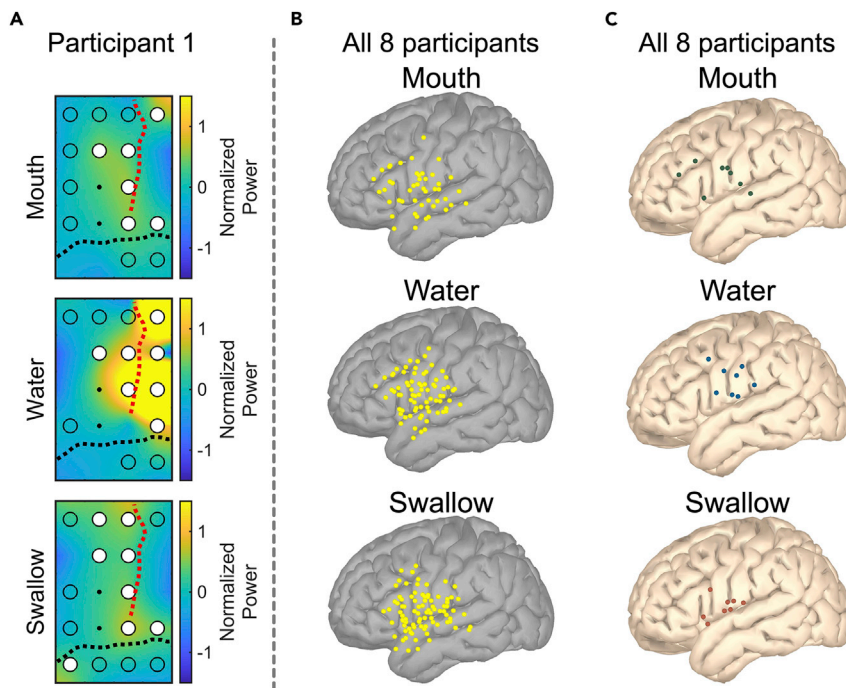
Figure 3. Distributions of high γ (HG) activities in the orofacial cortex

(A) The contour maps calculated from Participant 1 indicate distributions of HG normalize power within the mouth, water, and swallow triggers. The pattern of HG distributions varies among the three triggers. Significant power increasing is indicated as white filled circles (corrected p < 0.05, single-sided permutation test with Bonferroni correction). The central sulcus and the Sylvian fissure are indicated by red and black dashed lines, respectively. The left side of the contour maps corresponds to the anterior side of the brain. The location of the implanted electrode is shown in Figure 1.

(B) For each trigger group, contacts indicating significant power increases in the HG band of all eight participants are plotted over the left hemisphere of the Montreal Neurological Institute (MNI) brain.

(C) The contacts indicating the maximum values of significant HG power increase from each participant are plotted on the left hemisphere of the MNI normalized brain. Within each trigger, the contact groups were defined as a mouth contact group (Mouth group), a water contact group (Water group), and a swallow contact group (Swallow group), colored green, blue, and red, respectively. In B and C, the contacts attached to the right hemisphere are transposed to the left hemisphere.

Phase-based analysis

We calculated the mean vectors of the preferred phase of synchronization (SIp) during motor- and sensory-related SIm increase. Motor-related SIp involved in mouth movement and swallowing, the angle of the mean vector ranged from 0° to 45° (Figure 6A left and right panels); however, in sensory-related SIp involved in water injection, the angle of the mean vector was approximately 270° (−90°) (Figure 6A medial panel). We observed significant nonuniformity in all groups (c.p < 0.01, Rayleigh test with Bonferroni correction).

We showed the θ or α frequency oscillations of the θ or α phase (Figure 6B) and HG normalized amplitude tuned by the θ or α phase (Figure 6C) during motor- and sensory-related SIm increase. Demonstrating that HG amplitude is modulated at certain lower-frequency phases proves that the coupling phenomenon occurred and that SIm values do not achieve high values artificially. During motor-related SIm increases involved in mouth movement and swallowing, HG normalized amplitude achieved the peak around the trough of α oscillations (Figures 6B and 6C, left and right panels). On the contrary, at sensory-related SIm increase involved in water injection, HG normalized amplitude peaked at the peak of θ oscillations (Figures 6B and 6C, medial panels).

There were clear differences between motor-related and sensory-related HG amplitude tuning; during PAC, the motor-related HG amplitude was tuned by the trough of α oscillations and the sensory-related HG amplitude was tuned by the peak of θ oscillations.

Table 1. Clinical profiles

| Participant	Sex	Age	Diagnosis	Number of orofacial contacts (total contacts)	Number of swallowing instances	Number of mouth openings	Number of water injections	Handedness	MNI coordinate (X/Y/Z)		
									Mouth contact	Water contact	Swallow contact
P1	F	36	L TLE	18 (68)	31	31	31	R	−61.8/1.7/23.5	−63.3/−9.9/28.4	−62.8/−3.4/12.9
P2	F	30	L TLE	20 (84)	41	41	41	R	−60.0/−4.8/20.3	−59.6/−13.6/33.7	−60.1/−6.2/8.5
P3	F	18	R TLE	18 (55)	27	27	27	L	56.5/23.2/28.6	62.7/0.2/31.5	68.0/−13.8/12.7
P4	M	24	L TLE	15 (69)	34	34	34	R	−68.9/−19.2/6.4	−68.1/−23.1/22	−61.9/11.7/−3.7
P5	M	51	L TLE	20 (72)	38	38	38	R	−57.4/13.2/2.0	−61.4/4.4/14.9	−57.4/13.2/2.0
P6	M	28	R TLE	20 (96)	27	27	27	R	53.1/34.6/17.9	55.1/11.2/39.6	68.7/1.3/6.3
P7	M	20	L TLE	20 (94)	33	33	33	R	−62.2/−2.1/23.7	−65.2/−7.0/14.3	−65.2/−7.0/14.3
P8	F	15	L TLE	20 (68)	37	37	37	R	−67.7/−10.6/12.9	−67.7/−10.6/12.9	−62.2/10.8/22.4

M, male; F, female; R, right; L, left; TLE, temporal lobe epilepsy.

Correlation between HG power and PAC

Finally, we investigated the correlation between SIm and HG normalized power. Using the Mouth group with Mouth-T, Water group with Water-T, and Swallow group with Swallow-T, the dynamic changes of SIm and HG normalized power were displayed from before 1.5 s to after 0.5 s around each trigger (Figures 7A and 7B). The peaks of motor-related SIm were 0.6–0.7 s earlier than those of motor-related HG normalized power. Using total implanted contacts (151 contacts), sequential correlation coefficients (r) between SIm and HG normalized power were plotted (Figure 7C). We set the threshold of correlation coefficients that achieved 80% statistical power; the threshold was ±0.2. During motor-related SIm increase, no significant correlation was observed (Figure 7C, left and right panels, cyan mesh area); however, during the sensory-related HG burst, a positive correlation was observed (Figure 7C, medial panel, yellow mesh area). At the motor-related HG burst, there was no obvious correlation (Figure 7C, left and right panels, yellow mesh area).

We calculated the correlation coefficients in combination with sequential SIm and HG normalized power from −1.5 s to 0.5 s around each trigger using total 151 contacts and illustrated them as a matrix (Figure 7D). In Water-T, we observed an obvious positive correlation along the diagonal line from approximately −0.5 to 0.5 s, which corresponded to the time when HG normalized power increased (Figure 7D, medial panel, red dashed square). The pattern that SIm and HG normalized power in the same time zone had a positive correlation was not observed in Mouth-T and Swallow-T. In Mouth-T and Swallow-T, a positive correlation was temporarily observed (Figure 7D, left and right panels, red arrows).

Sensory-related PAC showed the positive correlation with sensory-related HG activities, whereas motor-related PAC has no obvious correlation with motor-related HG activities.
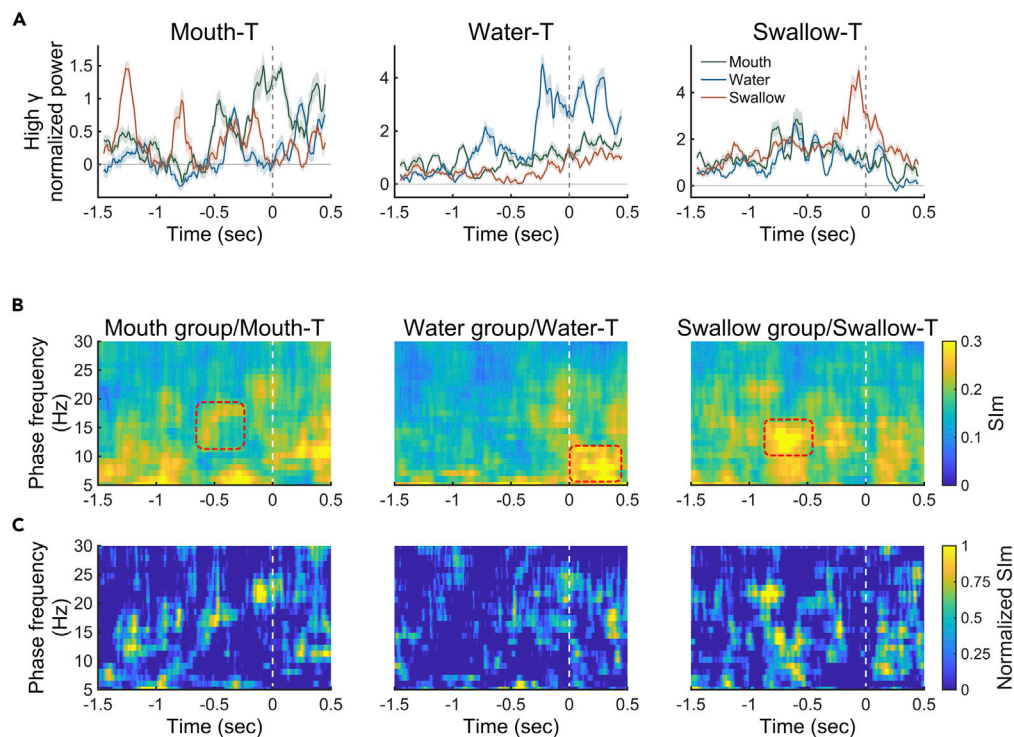
Figure 4. Temporal profile of high γ (HG) activities and phase-amplitude coupling (PAC)

(A) Averaged normalized power of HG calculated from the Mouth (green), Water (blue), and Swallow groups (red) are plotted from −1.5 to 0.5 s around Mouth-triggers (T), Water-T, and Swallow-T. At 0 s of Mouth-T, only the Mouth group showed an HG burst. At 0 s of Water-T, the Water group showed notable HG bursts. With Swallow-T, the Swallow group showed an increase in HG power. The error bars indicate 95% confidence intervals.

(B) For phase-amplitude coupling (PAC) analyses, the magnitudes of synchronization index (SIm) were calculated between lower-frequency (5–30 Hz, 1 Hz bin) phase (vertical axes) and HG (75–150 Hz) amplitude. We used the Mouth group in Mouth-T, Water group in Water-T, and Swallow group in Swallow-T. In motor-related PAC, including the Mouth group and Swallow group, high values of SIm were mainly observed before HG burst (red dashed square). On the contrary, in sensory-related PAC, including the Water group, high values of SIm were primarily observed during HG burst (red dashed square). The main lower-frequency band indicating high values of SIm was primarily under 20 Hz.

(C) Normalized SIm values are also shown. The patterns of high normalized SIm values were similar to that of high SIm values.

The Mouth, Water, and Swallow groups are shown in Figure 3C.

DISCUSSION

In this study, we hypothesized that the swallowing water task could demonstrate differences between motor and sensory neural processing because the swallowing task possesses two aspects, motor tasks represented by mouth opening and swallowing and a sensory task represented by water injection. Using intracranial electrodes over the orofacial cortex, we showed both motor- and sensory-related HG activities, and PAC occurred in a relationship with these HG activities. Moreover, PAC showed in the differences between motor- and sensory-related neural oscillations that motor-related HG activities are coupled with the α band (10–16 Hz) before motor-related HG power increases and, contrarily, sensory-related HG activities coupled with the θ band (5–9 Hz) during sensory-related HG power increase.

The cortex may trigger swallowing and modulate the brainstem (Ertekin and Aydogdu, 2003), and HG activities appeared in the cortex during the voluntary swallowing phase rather than during the involuntary swallowing phase (Hashimoto et al., 2021b). These findings support that the cooperation between voluntary and involuntary movements and the cortex and the brainstem is necessary for normal swallowing. Moreover, unimpaired sensory feedback is necessary for swallowing execution (Muhle et al., 2018), and the continuous sensory feedback from the oral cavity constantly modulates swallowing and results in the adaptation of the swallowing-related motor program to the bolus (Cook et al., 1989; Muhle et al., 2021). Therefore, the cooperation between sensory input
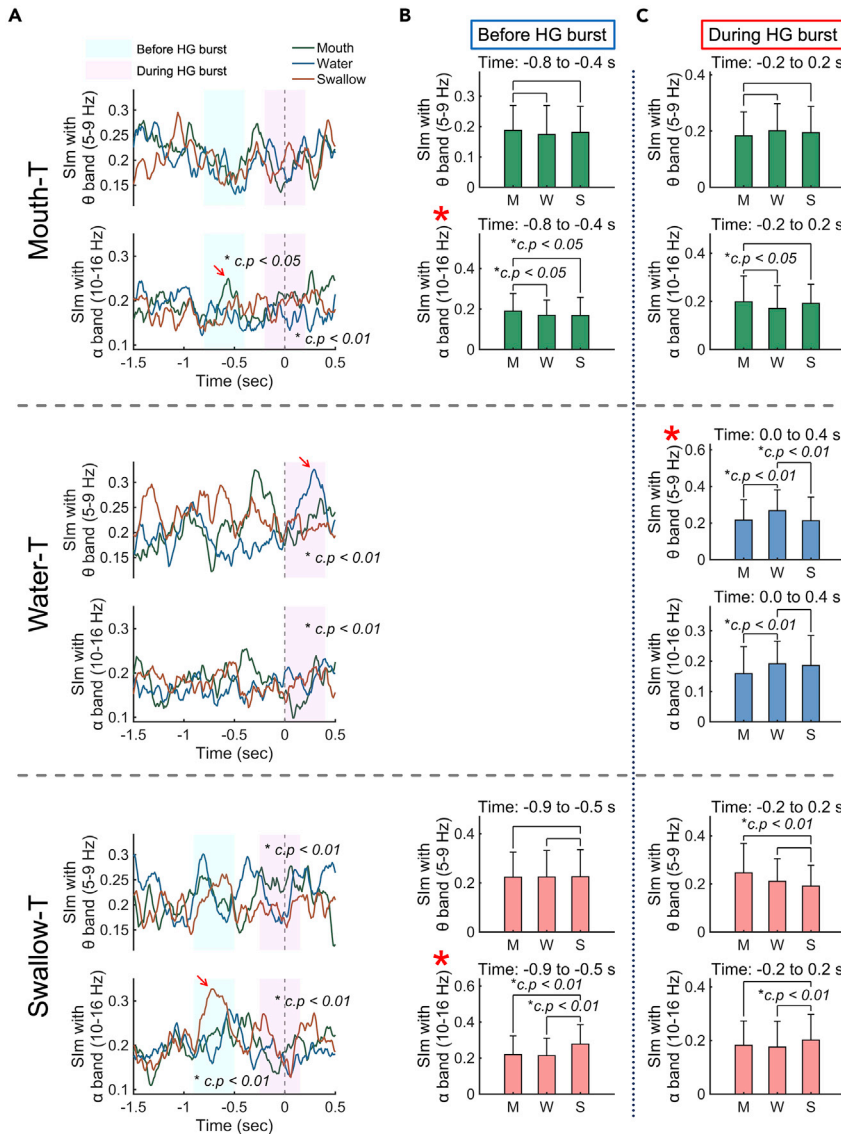
Figure 5. Motor-related phase-amplitude coupling (PAC) appeared before high γ (HG) burst, sensory-related PAC appeared during HG burst

(A) Dynamic changes of magnitudes of synchronization index (SIm) of θ band (5–9 Hz) and α band (10–16 Hz) coupled with HG are plotted among Mouth-triggers (T), Water-T, and Swallow-T. The results calculated from the Mouth, Water, and Swallow groups are indicated by green, blue, and red lines, respectively. The peaks of SIm are indicated by red arrows. The times before and during the HG burst are indicated as cyan and magenta mesh areas, respectively. We compared the three contact groups using one-way analysis of variance with Bonferroni correction. Significant corrected p values (c.p < 0.05 or c.p < 0.01) are indicated by a black star.

(B) The SIm values calculated from each group before HG burst are compared using a t test with Bonferroni correction. In Mouth-T, the α (10–16 Hz)-HG SIm of the Mouth group achieved significantly higher values than the other two groups, and in Swallow-T, the α-HG SIm of the Swallow group achieved significantly higher values rather than the other two groups (red asterisk).

(C) The SIm values during the HG burst were compared among the three groups by a t test with Bonferroni correction. In Water-T, the θ (5–9 Hz)-HG SIm of the Water group achieved significantly higher values than the other two groups (red asterisk). The error bars in (B) and (C) indicate the standard deviation. Significant differences (c.p < 0.05 or c.p < 0.01) were indicated by a black star.

M, Mouth contact group; W, Water contact group; S, Swallow contact group. These three groups are shown in Figure 3C.

Table 2. Main low-frequency band coupled with high γ amplitude

Event	Type	Before high γ burst	During high γ burst
Mouth opening	Motor	α band (10–16 Hz)	No significant coupling
Swallowing	Motor	α band (10–16 Hz)	No significant coupling
Water injection	Sensory	No significant coupling	θ Band (5–9 Hz)

and motor output is indispensable for swallowing, and this profile enabled us to demonstrate the differences between motor- and sensory-related neural oscillatory changes.

We used three different contact groups. Contacts related to mouth movement were primarily in the frontal lobe, including the lateral precentral gyrus and in the ventrolateral prefrontal cortex. These regions have been reported to be actively involved in orofacial motor action (Loh et al., 2020; Miller et al., 2007). Contacts related to water injection were observed in the lateral portion along the central sulcus, which were known to be activated by tactile stimulation of the buccal mucosa (Miyaji et al., 2014). Contacts related to swallowing were observed in regions along the Sylvian fissure that are activated by swallowing (Dziewas et al., 2003; Hamdy et al., 1999a; Lowell et al., 2008; Martin et al., 2004; Satow et al., 2004; Toogood et al., 2017). The distribution pattern of the contacts observed in this study was concordant with that reported previously. In another study, we reported the distribution and dynamic changes of cortical oscillations, including HG activities, in detail (Hashimoto et al., 2021b).

HG activities associated with hand movements were coupled with the α phase before the HG increase (Yanagisawa et al., 2012b); hence, a hold-and-release model of HG amplitude was proposed, which indicated that strong coupling restricted the HG activities and attenuation of the coupling releases the HG activities. The high-PAC state may suppress cortical information processing before movement onset, and its cessation may induce a shift to an active processing state (de Hemptinne et al., 2015). In this study, α-HG PAC related to mouth opening and swallowing was also observed before the HG burst. In a previous study, the maximum value of the motor-related HG amplitude was locked to the trough of the α oscillation (Yanagisawa et al., 2012b), whereas in our study, the HG amplitude associated with mouth opening and swallowing was also locked to the trough of the α oscillation. Our finding regarding motor-related PAC was similar to that of previous studies; therefore, we inferred that motor-related PAC in the orofacial cortex was successfully demonstrated by the mouth opening and swallowing tasks.

HG power is strongly correlated with neural firing rate (Ray et al., 2008), and neural spiking is locked to the trough of the α oscillations (Haegens et al., 2011). Therefore, during mouth opening- and swallowing-related α-HG PAC, the HG amplitude might be modulated by the trough of the α oscillations. Moreover, it has been proposed that α oscillations represented a pulsed inhibition of ongoing neural activity (Mathewson et al., 2011), and therefore, it may be reasonable that our results showed no HG activities during the appearance of motor-related α-HG coupling.

Previous studies have demonstrated that HG activities were induced by somatosensory stimulation (Hashimoto et al., 1996; Hirata et al., 2002; Muhle et al., 2021; Plenz and Kitai, 1996), whereas we showed the HG burst related to water injection. Sensory-related PAC was studied primarily using visual (Seymour et al., 2017; Voytek et al., 2010) or auditory tasks (Luo and Poeppel, 2007; Malinowska and Boatman-Reich, 2016); however, PAC studies using somatosensory stimulation are limited. In this study, during the sensory-related HG burst, the θ-HG PAC was observed, and its HG amplitude was locked to the peak of the θ oscillation, which is contrary to motor-related PAC.

EEG studies suggest that θ oscillations are related to both sensory and motor behaviors (Tomassini et al., 2017) and a general property of brain activity (Ramayya et al., 2020). In the epileptic brain, the hippocampal θ rhythm was increased (Kitchigina and Butuzova, 2009) and seizure-related HFA was coupled with θ band (Hashimoto et al., 2020b, 2021a). The θ oscillations are involved in both sensory and motor neural processing, and both physiological and pathological neural processing, and in this study, we provide a new insight into the sensory-related θ-HG coupling.

Epilepsy studies reported a positive correlation between coupling values and high-frequency amplitude (Hashimoto et al., 2021a; Weiss et al., 2016). We showed the continuous positive correlation between
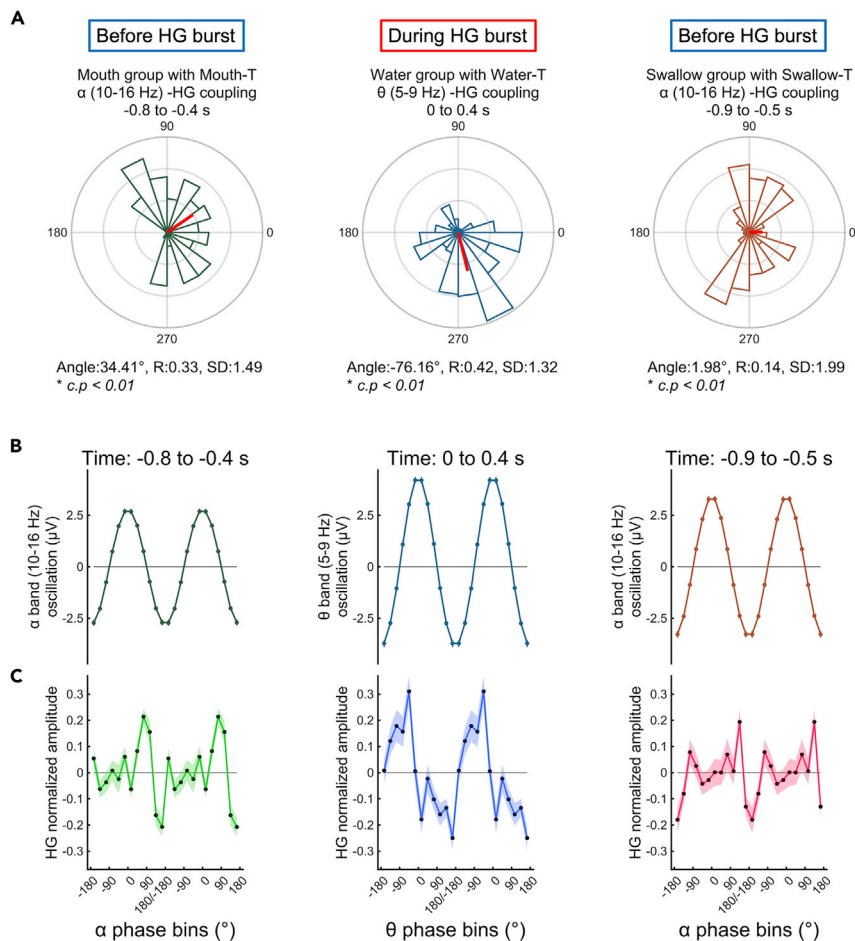
Figure 6. Mouth- and swallow-related high γ (HG) amplitudes were tuned by the trough of α (10–16 Hz) oscillations, and water-related HG amplitude was tuned by the peak of θ (5–9 Hz) oscillations

(A) We calculated average values of the preferred phase of synchronization (SIp) at the time when magnitudes of synchronization index (SIm) increased. Motor-related SIm calculated from the Mouth group with Mouth-triggers (T) and the Swallow group with Swallow-T increased before HG burst, and sensory-related SIm calculated from the Water group with Water-T increased during HG burst. The length and standard deviation of the mean vector are indicated as R and SD, and corrected p values (c.p) calculated by the Rayleigh test with Bonferroni correction are shown. The average angle of motor-related SIp approximately ranged from 0° to 45°; however, that of sensory-related SIp was approximately 270° (−90°). Significant c.ps are indicated by a black star.

When SIm increased, the lower-frequency oscillations of the lower-frequency phase (B) and HG normalized amplitude tuned by the lower-frequency phase (C) are displayed. In the Mouth and Swallow groups, the HG normalized amplitude peaked at the trough of α oscillation, and in the water group, the HG normalized amplitude peaked at the peak of θ oscillation. The error bars in (B) and (C) indicate 95% confidence intervals.

The Mouth, Water, and Swallow groups are shown in Figure 3C.

the θ-HG PAC and HG power related to sensory stimulation. We expected that motor-related α-HG PAC might correlate positively with the later HG power burst; contrary to our expectation, no obvious positive correlation was found; nonetheless, a positive correlation was temporally observed at approximately 0.3 s of Mouth-T (Figure 7D, left panel, red arrow). We inferred that this positive correlation was caused by sensory input since the water bolus was injected immediately after mouth opening.

In conclusion, we demonstrated the differences in PAC between the α (10–16 Hz) phase and HG amplitude appearing before the motor-related HG power burst and PAC between the θ (5–9 Hz) phase and HG amplitude appearing during the sensory-related HG burst. Moreover, we showed that, during the appearance of PAC, motor-related HG amplitudes were modulated at the trough of α oscillations and sensory-related HG amplitudes were modulated at the peak of θ oscillations. We inferred that these neuro-oscillatory
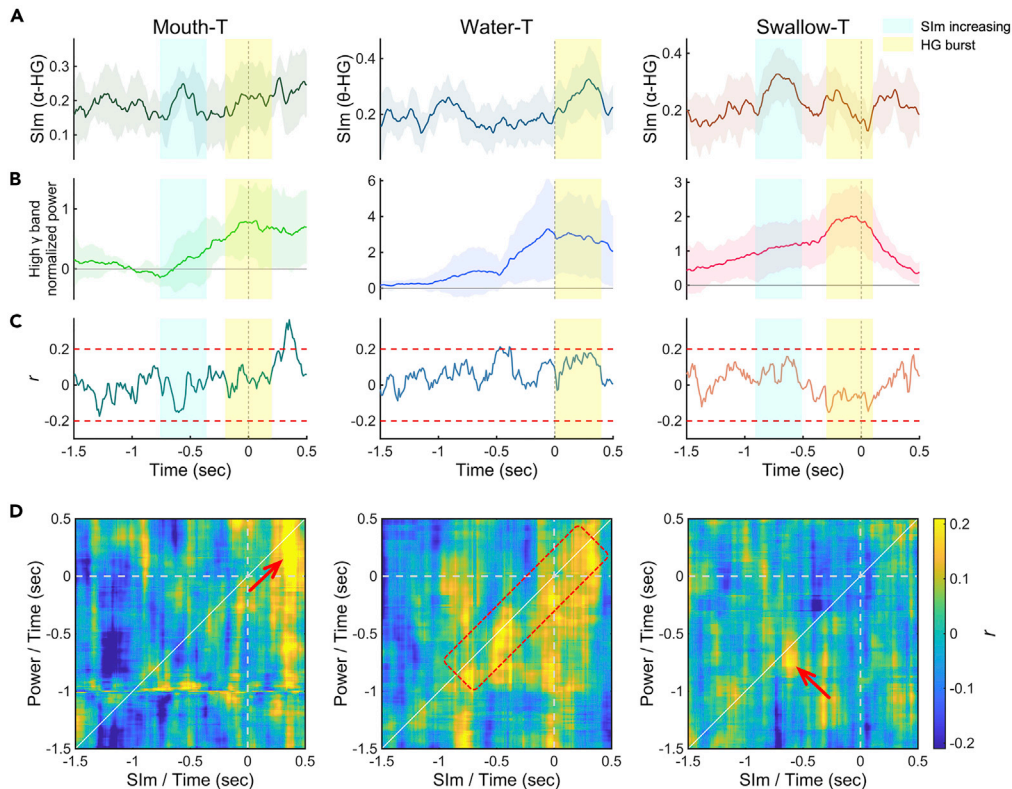
Figure 7. Sensory-related SIm positively correlated with high γ (HG) normalized power

(A–C)Using the Mouth group with Mouth-triggers (T), Water group with Water-T, and Swallow group with Swallow-T, dynamic changes of magnitudes of synchronization index (SIm) (A) and HG normalized power (B) were plotted from −1.5 to 0.5 s around each trigger. In the motor-related SIm of the Mouth and Swallow groups, SIm between α band (10–16 Hz) and HG was calculated, and in the sensory-related SIm of the Water group, SIm between θ band (5–9 Hz) and HG was also calculated. Using a total of 151 implanted contacts, we calculated sequential correlation coefficients (r) between SIm and HG normalized power (C). The time of the SIm increase and HG burst are indicated as cyan and yellow mesh areas, respectively. In the Water group, the SIm increase and HG burst co-occurred. The threshold of correlation coefficients that achieved 80% statistical power are indicated as red dashed lines (± 0.2).

(D) Using 151 total implanted contacts, correlation coefficients (r) are shown for all combinations of sequential SIm (horizontal axes) and sequential HG normalized power (vertical axes), from −1.5 to 0.5 s around each trigger. In the Water group, we observed a positive correlation along the diagonal line (red dashed square). In the Mouth and Swallow groups, a positive correlation was temporarily observed (red arrows). The error bars in (A) and (B) indicate 95% confidence intervals.

The Mouth, Water, and Swallow groups are shown in Figure 3C.

differences when coupling occurs, in the lower-frequency band, which coupled with HG amplitude, and in the lower-frequency phase, which modulates HG amplitude, may reflect the differences between motor- and sensory-related neural processing.

Limitations of the study

This study has a few limitations. First, we focused only on the orofacial cortex; multiple cortices are activated during swallowing (Ertekin and Aydogdu, 2003); however, our study could not demonstrate cortical activities other than in the orofacial region. Second, in this study, we divided swallowing events into three parts (mouth opening, water injection, and swallowing). The time of mouth opening and water injection were detected using the video captured by Kinect v2, having 30 frames per second; therefore, a maximum gap of 33 ms may occur. For more precise analysis, we must improve the detection methods of the time of mouth opening and water injection. Moreover, our method could not discriminate whether the sensory input occurred from the lip, the buccal mucosa, the tongue, or the pharynx. Third, we defined the θ band as 5–9 Hz and the α band as 10–16 Hz. However, the frequency ranges generally used are 4–8 Hz for the θ band (Canolty et al., 2006) and 8–14 Hz for the α band (Haegens et al., 2011). We set the frequency range in an effort to demonstrate that the frequency range in which

coupling occurred related to motor- and sensory-related tasks differ. Fourth, we focused only on frequencies ≥5 Hz. Since we used a 400-ms time window for SIm calculation, the minimum frequency in which at least two oscillation cycles were included was 5 Hz (Cohen, 2008). Fifth, we confirmed that all participants had normal swallowing function by medical interview. However, instrumental swallowing evaluation such as videoendoscopic evaluation or videofluoroscopy is needed for more precise and objective evaluation. Sixth, the age range of our study was relatively wide (15–51 years), and age-related changes in cortical activation related to swallowing have previously been described (Teismann et al., 2010). Therefore, there is a possibility that aging may influence our results. Seventh, there is a possibility that the sex may influence our results; however, our sample size is too small to comment on the differences between males and females. Finally, a hemispheric dominance for swallowing and the temporal sequence from one side to the other side has been reported (Dziewas et al., 2003; Malandraki et al., 2010; Mihai et al., 2014; Mosier et al., 1999; Teismann et al., 2009). Our dataset included two right hemispheres and six left hemispheres, and seven right-handed participants and one left-handed participant (Table 1). We think that our sample size is too small to comment on the hemispheric dominance for swallowing.

STAR★METHODS

Detailed methods are provided in the online version of this paper and include the following:

- KEY RESOURCES TABLE
- RESOURCE AVAILABILITY
  - Lead contact
  - Materials availability
  - Data and code availability
- EXPERIMENTAL MODEL AND SUBJECT DETAILS
  - Participants
- METHOD DETAILS
  - Intracranial electrodes
  - Electrode location
  - Task
  - Swallowing monitoring
  - Signal segmentation
  - Data acquisition and preprocessing
- QUANTIFICATION AND STATISTICAL ANALYSIS
  - HG power contour map
  - Extraction of contacts
  - Dynamic frequency power changes
  - Phase amplitude coupling analyses
  - Normalized SIm
  - Phase-conditioned analysis
  - Correlation analysis
  - Statistics

SUPPLEMENTAL INFORMATION

Supplemental information can be found online at https://doi.org/10.1016/j.isci.2021.102786.

AUTHOR CONTRIBUTIONS

Conceptualization, M.H.; methodology, H.H.; software, H.H.; formal analysis, H.H.; investigation, H.H., F.Y., H.M., and M.H.; resources, S.K., S.O., N.T., H.M.K., T. Yanagisawa, H.K., and M.H.; writing - original draft, H.H.; writing - review & editing, K.T. and M.H.; visualization, H.H.; supervision, T. Yoshimine, H.K., and M.H.; project administration, M.H.; funding acquisition, H.H. and M.H.

DECLARATION OF INTERESTS

The authors declare no competing interests.

REFERENCES

Amiri, M., Frauscher, B., and Gotman, J. (2019). Interictal coupling of HFO s and slow oscillations predicts the seizure-onset pattern in mesiotemporal lobe epilepsy. Epilepsia 60, 1160–1170.

Ayoubian, L., Lacoma, H., and Gotman, J. (2013). Automatic seizure detection in SEEG using high frequency activities in wavelet domain. Med. Eng. Phys. 35, 319–328.

Berens, P. (2009). CircStat: a MATLAB toolbox for circular statistics. J. Stat. Softw. 31, 1–21.

Canolty, R.T., Edwards, E., Dalal, S.S., Soltani, M., Nagarajan, S.S., Kirsch, H.E., Berger, M.S., Barbaro, N.M., and Knight, R.T. (2006). High gamma power is phase-locked to theta oscillations in human neocortex. Science 313, 1626–1628. https://doi.org/10.1126/science.1128115.

Cohen, M.X. (2008). Assessing transient cross-frequency coupling in EEG data. J. Neurosci. Methods 168, 494–499. https://doi.org/10.1016/j.jneumeth.2007.10.012.

Cook, I.J., Dodds, W.J., Dantas, R.O., Kern, M.K., Massey, B.T., Shaker, R., and Hogan, W.J. (1989). Timing of videofluoroscopic, manometric events, and bolus transit during the oral and pharyngeal phases of swallowing. Dysphagia 4, 8–15.

Crone, N.E., Miglioretti, D.L., Gordon, B., and Lesser, R.P. (1998a). Functional mapping of human sensorimotor cortex with electrocorticographic spectral analysis. II. Event-related synchronization in the gamma band. Brain 121 (Pt 12), 2301–2315.

Crone, N.E., Miglioretti, D.L., Gordon, B., Sieracki, J.M., Wilson, M.T., Uematsu, S., and Lesser, R.P. (1998b). Functional mapping of human sensorimotor cortex with electrocorticographic spectral analysis. I. Alpha and beta event-related desynchronization. Brain 121 (Pt 12), 2271–2299.

Cuellar, M., Harkrider, A., Jenson, D., Thornton, D., Bowers, A., and Saltuklaroglu, T. (2016). Time–frequency analysis of the EEG mu rhythm as a measure of sensorimotor integration in the later stages of swallowing. Clin. Neurophysiol. 127, 2625–2635.

Dalal, S.S., Guggisberg, A.G., Edwards, E., Sekihara, K., Findlay, A.M., Canolty, R.T., Berger, M.S., Knight, R.T., Barbaro, N.M., Kirsch, H.E., and Nagarajan, S.S. (2008). Five-dimensional neuroimaging: localization of the time-frequency dynamics of cortical activity. Neuroimage 40, 1686–1700. https://doi.org/10.1016/j.neuroimage.2008.01.023.

de Hemptinne, C., Swann, N.C., Ostrem, J.L., Ryapolova-Webb, E.S., San Luciano, M., Galifianakis, N.B., and Starr, P.A. (2015). Therapeutic deep brain stimulation reduces cortical phase-amplitude coupling in Parkinson's disease. Nat. Neurosci. 18, 779–786. https://doi.org/10.1038/nn.3997.

Dziewas, R., Sörös, P., Ishii, R., Chau, W., Henningsen, H., Ringelstein, E.B., Knecht, S., and Pantev, C. (2003). Neuroimaging evidence for cortical involvement in the preparation and in the act of swallowing. Neuroimage 20, 135–144.

Edakawa, K., Yanagisawa, T., Kishima, H., Fukuma, R., Oshino, S., Khoo, H.M., Kobayashi, M., Tanaka, M., and Yoshimine, T. (2016). Detection of epileptic seizures using phase-amplitude coupling in intracranial electroencephalography. Sci. Rep. 6, 25422. https://doi.org/10.1038/srep25422.

Ertekin, C., and Aydogdu, I. (2003). Neurophysiology of swallowing. Clin. Neurophysiol. 114, 2226–2244. https://doi.org/10.1016/s1388-2457(03)00237-2.

Firmin, H., Reilly, S., and Fourcin, A. (1997). Non-invasive monitoring of reflexive swallowing. J. Speech. Lang. Hear. Res. 10, 171–184.

Furlong, P.L., Hobson, A.R., Aziz, Q., Barnes, G.R., Singh, K.D., Hillebrand, A., Thompson, D.G., and Hamdy, S. (2004). Dissociating the spatio-temporal characteristics of cortical neuronal activity associated with human volitional swallowing in the healthy adult brain. Neuroimage 22, 1447–1455. https://doi.org/10.1016/j.neuroimage.2004.02.041.

Gow, D., Hobson, A.R., Furlong, P., and Hamdy, S. (2004). Characterising the central mechanisms of sensory modulation in human swallowing motor cortex. Clin. Neurophysiol. 115, 2382–2390. https://doi.org/10.1016/j.clinph.2004.05.017.

Haegens, S., Nácher, V., Luna, R., Romo, R., and Jensen, O. (2011). α-Oscillations in the monkey sensorimotor network influence discrimination performance by rhythmical inhibition of neuronal spiking. Proc. Natl. Acad. Sci. U S A 108, 19377–19382.

Hamdy, S., Aziz, Q., Rothwell, J.C., Singh, K.D., Barlow, J., Hughes, D.G., Tallis, R.C., and Thompson, D.G. (1996). The cortical topography of human swallowing musculature in health and disease. Nat. Med. 2, 1217–1224.

Hamdy, S., Mikulis, D.J., Crawley, A., Xue, S., Lau, H., Henry, S., and Diamant, N.E. (1999a). Cortical activation during human volitional swallowing: an event-related fMRI study. Am. J. Physiol. 277, G219–G225.

Hamdy, S., Rothwell, J.C., Brooks, D.J., Bailey, D., Aziz, Q., and Thompson, D.G. (1999b). Identification of the cerebral loci processing human swallowing with H2(15)O PET activation. J. Neurophysiol. 81, 1917–1926.

Hashimoto, H., Hasegawa, Y., Araki, T., Sugata, H., Yanagisawa, T., Yorifuji, S., and Hirata, M. (2017). Non-invasive detection of language-related prefrontal high gamma band activity with beamforming MEG. Sci. Rep. 7, 14262. https://doi.org/10.1038/s41598-017-14452-3.

Hashimoto, H., Hirata, M., Takahashi, K., Kameda, S., Katsuta, Y., Yoshida, F., Hattori, N., Yanagisawa, T., Palmer, J., Oshino, S., et al. (2018). Non-invasive quantification of human swallowing using a simple motion tracking system. Sci. Rep. 8, 5095. https://doi.org/10.1038/s41598-018-23486-0.

Hashimoto, H., Kameda, S., Maezawa, H., Oshino, S., Tani, N., Khoo, H.M., Yanagisawa, T., Yoshimine, T., Kishima, H., and Hirata, M. (2020a). A swallowing decoder based on deep transfer learning: AlexNet classification of the intracranial electrocorticogram. Int. J. Neural Syst. 0, 2050056. https://doi.org/10.1142/s0129065720500562.

Hashimoto, H., Khoo, H.M., Yanagisawa, T., Tani, N., Oshino, S., Kishima, H., and Hirata, M. (2020b). Coupling between infraslow activities and high-frequency oscillations precedes seizure onset. Epilepsia Open 5, 501–506. https://doi.org/10.1002/epi4.12425.

Hashimoto, H., Khoo, H.M., Yanagisawa, T., Tani, N., Oshino, S., Kishima, H., and Hirata, M. (2021a). Phase-amplitude coupling of ripple activities during seizure evolution with theta phase. Clin. Neurophysiol. 132, 1243–1253. https://doi.org/10.1016/j.clinph.2021.03.007.

Hashimoto, H., Takahashi, K., Kameda, S., Yoshida, F., Maezawa, H., Oshino, S., Tani, N., Khoo, H.M., Yanagisawa, T., Yoshimine, T., et al. (2021b). Swallowing-related neural oscillation: an intracranial EEG study. Ann. Clin. Transl. Neur. 8, 1224–1238. https://doi.org/10.1002/acn3.51344.

Hashimoto, I., Mashiko, T., and Imada, T. (1996). Somatic evoked high-frequency magnetic oscillations reflect activity of inhibitory interneurons in the human somatosensory cortex. Electroencephalogr. Clin. Neurophysiol. 100, 189–203.

Hirata, M., Kato, A., Taniguchi, M., Ninomiya, H., Cheyne, D., Robinson, S.E., Maruno, M., Kumura, E., Ishii, R., Hirabuki, N., et al. (2002). Frequency-dependent spatial distribution of human somatosensory evoked neuromagnetic fields. Neurosci. Lett. 318, 73–76.

Jacobs, J., LeVan, P., Châtillon, C.-É., Olivier, A., Dubeau, F., and Gotman, J. (2009). High frequency oscillations in intracranial EEGs mark epileptogenicity rather than lesion type. Brain 132, 1022–1037.

Jean, A. (2001). Brain stem control of swallowing: neuronal network and cellular mechanisms. Physiol. Rev. 81, 929–969.

Kitchigina, V.F., and Butuzova, M.V. (2009). Theta activity of septal neurons during different epileptic phases: the same frequency but different significance? Exp. Neurol. 216, 449–458.

Kober, S.E., and Wood, G. (2014). Changes in hemodynamic signals accompanying motor imagery and motor execution of swallowing: a near-infrared spectroscopy study. Neuroimage 93 (Pt 1), 1–10. https://doi.org/10.1016/j.neuroimage.2014.02.019.

Kusuhara, T., Nakamura, T., Shirakawa, Y., Mori, K., Naomoto, Y., and Yamamoto, Y. (2004). Impedance pharyngography to assess swallowing function. J. Int. Med. Res. 32, 608–616.

Lakatos, P., Karmos, G., Mehta, A.D., Ulbert, I., and Schroeder, C.E.J.s. (2008). Entrainment of neuronal oscillations as a mechanism of attentional selection. Science 320, 110–113.

Loh, K.K., Procyk, E., Neveu, R., Lamberton, F., Hopkins, W.D., Petrides, M., and Amiez, C. (2020). Cognitive control of orofacial motor and vocal responses in the ventrolateral and dorsomedial human frontal cortex. Proc. Natl. Acad. Sci. U S A 117, 4994–5005.

Lowell, S.Y., Poletto, C.J., Knorr-Chung, B.R., Reynolds, R.C., Simonyan, K., and Ludlow, C.L. (2008). Sensory stimulation activates both motor and sensory components of the swallowing system. Neuroimage 42, 285–295. https://doi.org/10.1016/j.neuroimage.2008.04.234.

Luo, H., and Poeppel, D.J.N. (2007). Phase patterns of neuronal responses reliably discriminate speech in human auditory cortex. Neuron 54, 1001–1010.

Maezawa, H., Yoshida, K., Nagamine, T., Matsubayashi, J., Enatsu, R., Bessho, K., and Fukuyama, H. (2008). Somatosensory evoked magnetic fields following electric tongue stimulation using pin electrodes. Neurosci. Res. 62, 131–139. https://doi.org/10.1016/j.neures.2008.07.004.

Malandraki, G.A., Sutton, B.P., Perlman, A.L., and Karampinos, D.C. (2010). Age-related differences in laterality of cortical activations in swallowing. Dysphagia 25, 238–249.

Malinowska, U., and Boatman-Reich, D. (2016). Cross-frequency coupling during auditory perception in human cortex. Annu. Int. Conf. IEEE Eng. Med. Biol. Soc. 2016, 5521–5524. https://doi.org/10.1109/EMBC.2016.7591977.

Maris, E., and Oostenveld, R. (2007). Nonparametric statistical testing of EEG- and MEG-data. J. Neurosci. Methods 164, 177–190. https://doi.org/10.1016/j.jneumeth.2007.03.024.

Mårnsson, I., and Sandberg, N. (1974). Effects of surface anesthesia on deglutition in man. Laryngoscope 84, 427–437.

Martin, R.E., MacIntosh, B.J., Smith, R.C., Barr, A.M., Stevens, T.K., Gati, J.S., and Menon, R.S. (2004). Cerebral areas processing swallowing and tongue movement are overlapping but distinct: a functional magnetic resonance imaging study. J. Neurophysiol. 92, 2428–2443. https://doi.org/10.1152/jn.01144.2003.

Mathewson, K.E., Lleras, A., Beck, D.M., Fabiani, M., Ro, T., and Gratton, G. (2011). Pulsed out of awareness: EEG alpha oscillations represent a pulsed-inhibition of ongoing cortical processing. Front. Psychol. 2, 99.

Matsumoto, A., Brinkmann, B.H., Matthew Stead, S., Matsumoto, J., Kucewicz, M.T., Marsh, W.R., Meyer, F., and Worrell, G. (2013). Pathological and physiological high-frequency oscillations in focal human epilepsy. J. Neurophysiol. 110, 1958–1964.

Mihai, P.G., Otto, M., Platz, T., Eickhoff, S.B., and Lotze, M. (2014). Sequential evolution of cortical activity and effective connectivity of swallowing using fMRI. Hum. Brain Mapp. 35, 5962–5973. https://doi.org/10.1002/hbm.22597.

Miller, K.J., Leuthardt, E.C., Schalk, G., Rao, R.P., Anderson, N.R., Moran, D.W., Miller, J.W., and Ojemann, J.G. (2007). Spectral changes in cortical surface potentials during motor movement. J. Neurosci. 27, 2424–2432. https://doi.org/10.1523/JNEUROSCI.3886-06.2007.

Miyaji, H., Hironaga, N., Umezaki, T., Hagiwara, K., Shigeto, H., Sawatsubashi, M., Tobimatsu, S., and Komune, S. (2014). Neuromagnetic detection of the laryngeal area: sensory-evoked fields to air-puff stimulation. Neuroimage 88, 162–169. https://doi.org/10.1016/j.neuroimage.2013.11.008.

Mosier, K.M., Liu, W.-C., Maldjian, J.A., Shah, R., and Modi, B. (1999). Lateralization of cortical function in swallowing: a functional MR imaging study. Am. J. Neuroradiol. 20, 1520–1526.

Muhle, P., Labeit, B., Wollbrink, A., Claus, I., Warnecke, T., Wolters, C.H., Gross, J., Dziewas, R., and Suntrup-Krueger, S. (2021). Targeting the sensory feedback within the swallowing network—reversing artificially induced pharyngolaryngeal hypesthesia by central and peripheral stimulation strategies. Hum. Brain Mapp. 42, 427–438.

Muhle, P., Suntrup-Krueger, S., and Dziewas, R. (2018). Neurophysiological adaptation and neuromodulatory treatment approaches in patients suffering from post-stroke dysphagia. Curr. Phys. Med. Rehabil. Rep. 6, 227–238.

Pfurtscheller, G. (1981). Central beta rhythm during sensorimotor activities in man. Electroencephalogr. Clin. Neurophysiol. 51, 253–264.

Pfurtscheller, G., and Aranibar, A. (1979). Evaluation of event-related desynchronization (ERD) preceding and following voluntary self-paced movement. Electroencephalogr. Clin. Neurophysiol. 46, 138–146.

Pipa, G., Stadtler, E.S., Rodriguez, E.F., Waltz, J.A., Muckli, L.F., Singer, W., Goebel, R., and Munk, M.H. (2009). Performance- and stimulus-dependent oscillations in monkey prefrontal cortex during short-term memory. Front. Integr.

Neurosci. 3, 25. https://doi.org/10.3389/neuro.07.025.2009.

Plenz, D., and Kitai, S.T. (1996). Generation of high-frequency oscillations in local circuits of rat somatosensory cortex cultures. J. Neurophysiol. 76, 4180–4184.

Ramayya, A.G., Yang, A.I., Buch, V.P., Burke, J.F., Richardson, A.G., Brandon, C., Stein, J.M., Davis, K.A., Chen, H.I., Proekt, A., et al. (2020). Theta synchrony is increased near neural populations that are active when initiating instructed movement. eNeuro 8. .ENEURO.0252-0220.2020. https://doi.org/10.1523/eneuro.0252-20.2020.

Ramos-Murguialday, A., Broetz, D., Rea, M., Läer, L., Yilmaz, Ö., Brasil, F.L., Liberati, G., Curado, M.R., Garcia-Cossio, E., and Vyziotis, A. (2013). Brain–machine interface in chronic stroke rehabilitation: a controlled study. Ann. Neurol. 74, 100–108.

Ray, S., Crone, N.E., Niebur, E., Franaszczuk, P.J., and Hsiao, S.S. (2008). Neural correlates of high-gamma oscillations (60–200 Hz) in macaque local field potentials and their potential implications in electrocorticography. J. Neurosci. 28, 11526–11536.

Salmelin, R., and Sams, M. (2002). Motor cortex involvement during verbal versus non-verbal lip and tongue movements. Hum. Brain Mapp. 16, 81–91.

Satow, T., Ikeda, A., Yamamoto, J., Begum, T., Thuy, D.H., Matsuhashi, M., Mima, T., Nagamine, T., Baba, K., Mihara, T., et al. (2004). Role of primary sensorimotor cortex and supplementary motor area in volitional swallowing: a movement-related cortical potential study. Am. J. Physiol. Gastrointest. Liver Physiol. 287, G459–G470. https://doi.org/10.1152/ajpgi.00323.2003.

Seymour, R.A., Rippon, G., and Kessler, K. (2017). The detection of phase Amplitude coupling during sensory processing. Front. Neurosci. 11, 487.

Shindo, K., Kawashima, K., Ushiba, J., Ota, N., Ito, M., Ota, T., Kimura, A., and Liu, M. (2011). Effects of neurofeedback training with an electroencephalogram-based brain–computer interface for hand paralysis in patients with chronic stroke: a preliminary case series study. J. Rehabil. Med. 43, 951–957.

Taylor, K., Mandon, S., Freiwald, W.A., and Kreiter, A.K. (2005). Coherent oscillatory activity in monkey area v4 predicts successful allocation of attention. Cereb. Cortex 15, 1424–1437. https://doi.org/10.1093/cercor/bhi023.

Teismann, I.K., Dziewas, R., Steinstraeter, O., and Pantev, C. (2009). Time-dependent hemispheric shift of the cortical control of volitional swallowing. Hum. Brain Mapp. 30, 92–100. https://doi.org/10.1002/hbm.20488.

Teismann, I.K., Steinstraeter, O., Schwindt, W., Ringelstein, E.B., Pantev, C., and Dziewas, R. (2010). Age-related changes in cortical swallowing processing. Neurobiol. Aging 31, 1044–1050. https://doi.org/10.1016/j.neurobiolaging.2008.07.001.

Tomassini, A., Ambrogioni, L., Medendorp, W.P., and Maris, E. (2017). Theta oscillations locked to

intended actions rhythmically modulate perception. Elife 6, e25618.

Toogood, J.A., Smith, R.C., Stevens, T.K., Gati, J.S., Menon, R.S., Theurer, J., Weisz, S., Affoo, R.H., and Martin, R.E. (2017). Swallowing preparation and execution: insights from a delayed-response functional magnetic resonance imaging (fMRI) study. Dysphagia 32, 526–541. https://doi.org/10.1007/s00455-017-9794-2.

Voytek, B., Canolty, R.T., Shestyuk, A., Crone, N.E., Parvizi, J., and Knight, R.T. (2010). Shifts in gamma phase-amplitude coupling frequency from theta to alpha over posterior cortex during visual tasks. Front. Hum. Neurosci. 4, 191. https://doi.org/10.3389/fnhum.2010.00191.

Weiss, S.A., Orosz, I., Salamon, N., Moy, S., Wei, L., Van't Klooster, M.A., Knight, R.T., Harper, R.M., Bragin, A., and Fried, I. (2016). Ripples on spikes show increased phase-amplitude coupling in mesial temporal lobe epilepsy seizure-onset zones. Epilepsia 57, 1916–1930.

Yanagisawa, T., Hirata, M., Saitoh, Y., Goto, T., Kishima, H., Fukuma, R., Yokoi, H., Kamitani, Y., and Yoshimine, T. (2011). Real-time control of a prosthetic hand using human electrocorticography signals. J. Neurosurg. 114, 1715–1722. https://doi.org/10.3171/2011.1.Jns101421.

Yanagisawa, T., Hirata, M., Saitoh, Y., Kishima, H., Matsushita, K., Goto, T., Fukuma, R., Yokoi, H., Kamitani, Y., and Yoshimine, T. (2012a). Electrocorticographic control of a prosthetic arm in paralyzed patients. Ann. Neurol. 71, 353–361. https://doi.org/10.1002/ana.22613.

Yanagisawa, T., Yamashita, O., Hirata, M., Kishima, H., Saitoh, Y., Goto, T., Yoshimine, T., and Kamitani, Y. (2012b). Regulation of motor representation by phase-amplitude coupling in the sensorimotor cortex. J. Neurosci. 32, 15467–15475. https://doi.org/10.1523/Jneurosci.2929-12.2012.

Yang, H., Guan, C., Chua, K.S., Chok, S.S., Wang, C.C., Soon, P.K., Tang, C.K., and Ang, K.K. (2014). Detection of motor imagery of swallow EEG signals based on the dual-tree complex wavelet transform and adaptive model selection. J. Neural Eng. 11, 035016. https://doi.org/10.1088/1741-2560/11/3/035016.

STAR★METHODS

KEY RESOURCES TABLE

REAGENT or RESOURCE	SOURCE	IDENTIFIER
Biological samples		
Intracranial electrodes	Unique Medical	https://www.unique-medical.jp
Electroglottograph	Laryngograph	http://www.laryngograph.com/index.html
Microphone / Swallowing sound, Inkou mike; SH-12iK	NANZU	https://www.nanzu.jp/syohin/mic-sh12ik.htm
Motion-tracking system using Kinect v2 (Microsoft)	Hashimoto et al. (2018)	https://doi.org/10.1038/s41598-018-23486-0
128-channel digital EEG system, EEG 2000	Nihon Kohden Corporation	https://www.nihonkohden.com
Software and algorithms		
FreeSurfer version 6	FreeSurfer	https://surfer.nmr.mgh.harvard.edu
Brainstorm software	Brainstorm	https://neuroimage.usc.edu/brainstorm/Introduction
EEGLAB version 14.1.2b	Swartz center for computational neuroscience	https://sccn.ucsd.edu/eeglab/index.php
Circular Statistics Toolbox	Philipp Berens	https://jp.mathworks.com/matlabcentral/fileexchange/10676-circular-statistics-toolbox-directional-statistics
BESA Research 6.0 software	BESA GmbH	https://www.besa.de
MATLAB R2020a	MathWorks	https://www.mathworks.com/?s_tid=gn_logo
Other		
Electric stimulator / NS-101	Unique Medical	https://www.unique-medical.jp

RESOURCE AVAILABILITY

Lead contact

Further information and requests for resources should be directed to and will be fulfilled by the Lead Contact, Masayuki Hirata (mhirata@ndr.med.osaka-u.ac.jp).

Materials availability

This study did not generate new unique reagents or materials.

Data and code availability

Original/source data in this study is available upon request. No unique code was generated in this study. Any additional information required to reanalyze the data reported in this study is available from the lead contact upon request.

EXPERIMENTAL MODEL AND SUBJECT DETAILS

Participants

Eight patients with intractable temporal lobe epilepsy participated in this study (four females, 15–51 years of age; mean and standard deviation (SD) of age 27.8 ± 11.6 years) (Table 1), and the patient group in this study was the same group used in our other published study (Hashimoto et al., 2020a, 2021b). They were admitted to Osaka University Hospital from April 2015 to July 2019 and underwent intracranial electrodes placement for intracranial electroencephalogram (iEEG) study. They had normal swallowing function, which was confirmed by a medical interview. All participants or their guardians were informed of this study's purpose and possible consequences, and written informed consent was obtained. The Ethics Committee of Osaka University Hospital approved this study (Nos. 08061, 16469).

METHOD DETAILS

Intracranial electrodes

Different types of electrodes (Unique Medical Co. Ltd., Tokyo, Japan), including grid, strip, and depth types, were implanted in the subdural space during conventional craniotomy as a clinical epileptic surgery. For analysis, we chose planar-surface platinum grid electrodes (4×5 contacts array) that were placed over the lateral portion of the central sulcus corresponding to the orofacial cortex. The number of total implanted contacts and selected contacts in each participant are shown in Table 1. The diameter of the contacts was 3 or 5 mm, and the intercontact center-to-center distance was 5, 7, or 10 mm.

Electrode location

Preoperative structural MRI was obtained with a 1.5-T or 3.0-T MRI scanner, and postoperative computed tomography (CT) scans were acquired with the implanted electrodes in place. The implanted electrodes that were obtained from the CT images were overlaid onto the 3-dimensional brain renderings from the MRI volume that was created by FreeSurfer software (https://surfer.nmr.mgh.harvard.edu). We obtained the Montreal Neurological Institute (MNI) coordinates of the implanted contacts with Brainstorm software (http://neuroimage.usc.edu/brainstorm/), which merged the preoperative MRI scans and postoperative CT scans. The location of the implanted electrodes that was visualized by Brainstorm (Figure 1) was then confirmed by intraoperative photographs.

Task

The experiments were performed approximately 1 week after surgical electrode placement when all participants fully recovered from surgery. The participants were asked to sit on a chair and to remain still, especially without moving their mouths. The participants then opened their mouths, and the examiner injected 2 mL of water into their mouths with a syringe. The tip of a syringe was put on the lip, participants closed their mouths, and the syringe was fixed. Next, the examiner injected a water bolus into the oral cavity. We inferred that sensory input from the oral cavity might occur; however, we could not individually stimulate the tongue, the buccal mucosa, or the pharynx by our method. We requested that the participants swallow the water bolus at their own pace without external cueing to prevent erroneous volitional water swallowing (aspiration). After we confirmed that the participants had completed one swallowing movement, the next water bolus was injected.

We planned to inject the water bolus approximately 50 times per participant; however, actual swallowing instances could not be achieved in some participants because of their fatigue. Moreover, some swallowing was excluded from analyses because of coughing or obscure swallowing. The number of swallowing instances are shown in Table 1 (27–41 times; mean and SD 33.5 ± 5.1 times).

Swallowing monitoring

For noninvasive swallowing detection, we used an electroglottograph (EGG), a microphone, and a motion-tracking system (Figure 2A). A laryngograph (Laryngograph Ltd, London, UK) was used as an EGG and recorded the neck impedance changes associated with swallowing (Firmin et al., 1997) (Figure 2B). A pair of contacts was placed on the neck skin below the thyroid cartilage of the participants at an intercontact center-to-center distance of 25 mm and was held in place by an elastic band.

Sounds of swallowing due to the bolus passing through the pharynx were detected by a throat microphone (Kusuhara et al., 2004) (Figure 2C). We connected the throat microphone (Inkou mike; SH-12iK, NANZU, Shizuoka, Japan) to the laryngograph to record the swallowing sounds. The shape of the microphone was arched to fit around the participant's neck. The sampling rate of a laryngograph and a throat microphone was 24,000 Hz.

We captured the motion of the participants at 30 frames per second with the motion-tracking system, which was newly developed by us using Kinect v2 (Microsoft, Redmond, Washington, USA) (Hashimoto et al., 2018). The participants were seated facing Kinect v2, which was placed on a tripod at a distance of one meter, and their mouth and throat movements were captured automatically.

An electric stimulator (NS-101; Unique Medical, Tokyo, Japan) supplied digital synchronizing signals to the laryngograph and a 128-channel digital EEG system. The signals made an LED light flash, which was captured by the RGB camera of Kinect v2. The digital triggers and LED light flash enabled us to synchronize

the multimodal data of an EGG, a microphone, the video captured by the RGB camera, and an intracranial EEG. The multimodal data enabled us to noninvasively monitor the swallowing movements. The video captured by the RGB camera enabled us to the detect time when the participants opened their mouths and when the water bolus was injected into the mouth.

Signal segmentation

The swallowing onset time was determined at the time when the impedance waveform reached the peak (Figure 2B). Swallowing sounds occurred frequently as the bolus of water passed through the pharynx (Kusuhara et al., 2004), and their evaluation in conjunction with the EGG helped us to judge whether the impedance change was caused by swallowing (Figure 2C). Additionally, we confirmed that the changes in impedance and sounds corresponded to water swallowing by using the video captured by the RGB camera. We inserted swallowing triggers, which corresponded to the swallowing onset time, into the iEEG data.

We could also detect the time when the participant opened his/her mouth and when the examiner injected water into the participants' mouth using the video captured by the RGB camera. Mouth triggers and water triggers, which corresponded to different times, were also inserted into iEEG data (the number of each trigger is shown in Table 1).

Data acquisition and preprocessing

The iEEG signals were measured with a 128-channel digital EEG system (EEG 2000; Nihon Kohden Corporation, Tokyo, Japan) and digitized at a sampling rate of 1000 Hz. BESA Research 6.0 software (BESA GmbH, Grafelfing, Germany) preprocessed the raw signals using a high-cut filter at 333 Hz to prevent aliasing and a 60-Hz notch filter to eliminate the alternating current line artifact, and the software exported the data as a text file. This text file containing iEEG signals was imported into MATLAB R2020a (MathWorks, Natick, MA, USA). Before any further processing, contacts containing external noise or epileptic discharge were excluded from further analyses. The iEEG signals were digitally re-referenced to a common average of implanted total contacts in each participant. We analyzed the iEEG signals that were time-locked to the triggers.

Throughout the following analyses, a bandpass filter using a two-way least-squares finite impulse response filter (pop_eegfiltnew.m from the EEGLAB version 14.1.2b, https://sccn.ucsd.edu/eeglab/index.php) was applied to the iEEG signals. To prevent edge-effect artifacts, additional 250 msec data remained at the initial and end points of the pre bandpass filtered signals. After bandpass filtering, the 250 msec extra data were excluded. For assessment of filtered signals, we showed θ (5-9 Hz), α (10-16 Hz), and high γ (HG) (75-150 Hz) filtered iEEG signals for one contact per one participant from all 8 patients, which were time-locked to each trigger (Figure S1).

QUANTIFICATION AND STATISTICAL ANALYSIS

HG power contour map

To create power contour maps, the power of each contact was constructed from the preprocessed iEEG signal by using a bandpass filter of HG band (75–150 Hz) in combination with the Hilbert transformation (Cohen, 2008). We calculated the averaged power during 0.5 s time-window, and the averaged power was normalized with the mean and SD of the power during -5.0 to -4.5 s of the swallowing triggers.

Extraction of contacts

Significant HG power increasing contacts (single-sided permutation tests with Bonferroni correction) were plotted over the left hemisphere of MNI normalized brain using Brainstorm software. The contacts attached to the right hemisphere were transposed to the left hemisphere.

The contacts indicating the maximum values of the significant HG power increase in the mouth, water, and swallow triggers were extracted from each participant; in total, eight contacts within each trigger were plotted on the left hemisphere of MNI normalized brain. These group of contacts associated with each trigger were defined as the Mouth, Water, and Swallow groups.

Dynamic frequency power changes

We obtained averaged power waveforms of the Mouth, Water, and Swallow groups relative to each trigger (mouth triggers, Mouth T; water triggers, Water T; swallowing triggers, Swallow T) in each HG band. A

power time series were constructed from a bandpass filtered signal in combination with the Hilbert transformation (Cohen, 2008). The power time series were normalized by the power from base-time (-1.0 s of Mouth T). Averaged frequency power values were calculated from a 100 (Figure 4A) or 400 msec (Figure 7B) time-window, which was shifted every 10 msec.

Phase amplitude coupling analyses

A synchronization index (SI) (Cohen, 2008) was used to measure the strength of coupling between the HG amplitude and lower frequency phase. Hilbert transformation was performed on the bandpass-filtered signals to obtain complex-valued analytic signals [Z(t)]. The amplitude [A(t)] and phase [ϕ(t)] were calculated from the complex-valued signals using Equation 1.

$$Z(t) = A\ (t) \cdot \ \exp(i\ \varphi\ (t)) \qquad \text{(Equation 1)}$$

The lower frequency phase was calculated using the angle of the Hilbert transformation in the bandpass-filtered signal. The center of a bandpass filter was shifted every 1 Hz from 5-30 Hz, and the width of the bandpass filter was $\pm$ 2.5 Hz. The HG amplitude was calculated using the squared magnitude of the Hilbert transformation in the 75–150 Hz bandpass filtered signal. Then, the phase of this amplitude was computed using the Hilbert transformation. The SI was calculated using Equation Equation 2.

$$SI = \frac{1}{n} \times \sum_{t=1}^{n} e^{i}[\varphi_{ISA}(t) - \varphi_{HFA}(t)] \qquad \text{(Equation 2)}$$

where "n" is the number of data points. We used a 400 ms time-window at a sampling rate of 1,000 Hz; therefore, the "n" value was 400. Since we used a 400 ms time-window, the minimum frequency in which at least two oscillation cycles were included was 5 Hz.

Since SI is a complex number, we used the magnitude of SI (SIm) in our calculations. SIm varies between 0 and 1, with 0 indicating completely desynchronized phases and 1 indicating perfectly synchronized phases.

The preferred phase of synchronization (SIp) was calculated by the arctan (image [SI] / real [SI]). SIp varies between -180° and +180°.

Normalized SIm

The boot-strapping technique was used (Cohen, 2008). The phase time series of high-frequency power amplitude is shifted in time by some random amount, and boot-strapping SIm (SImb) is calculated with the lower frequency phase. This procedure was repeated 400 times to create a distribution of SImb. The normalized SIm was calculated using the mean and SD of the distribution of SImb.

Phase-conditioned analysis

We calculated the mean vector (angle and length) using the Circular Statistics Toolbox (Berens, 2009). To identify the lower frequency phase to which the HG amplitude was coupled, we calculated the average oscillations of lower frequency band and the normalized amplitude of HG band within each lower frequency band phase bin of 30°: -180° – -150°, -150° – -120°, …, and 150° – 180°.

Correlation analysis

Using all the implanted contacts (total 151 contacts), we calculated Pearson correlation coefficients between SIm and the HG normalized power. The values greater than +3 SD or less than -3 SD were excluded as outliers. Using the Monte Carlo method, we set the threshold of correlation coefficients that achieved 80% statistical power.

Statistics

We used a permutation test for the statistical evaluation of HG power changes (Maris and Oostenveld, 2007). For comparison of two groups, a T-test was used. For the correction of multiple comparisons, we used a Bonferroni correction. To compare three groups of mouth triggers, water triggers, and swallowing triggers, we used one-way analysis of variance (ANOVA). We performed the Rayleigh test to evaluate the nonuniformity of SIp using the Circular Statistics Toolbox(Berens, 2009).